

Thiolation and PEGylation of silicon carbide nanoparticles

Péter Rózsa^{a,b}, Olga Krafcsik^{c,d}, Zsolt Czigány^d, Sándor Lenk^c, David Beke^{b,e}, Adam Gali^{b,c,f,*}

^aHevesy György PhD School of Chemistry, Eötvös Loránd University, Pázmány Péter sétány 1/A, H-1117 Budapest, Hungary

^bHUN-REN Wigner Research Centre for Physics, Institute for Solid State Physics and Optics, P.O. Box 49, H-1525 Budapest, Hungary

^cDepartment of Atomic Physics, Institute of Physics, Budapest University of Technology and Economics, Műegyetem rakpart 3., H-1111, Budapest, Hungary

^dHUN-REN Centre for Energy Research, Institute of Technical Physics and Materials Science, P.O. Box 49, H-1525, Budapest, Hungary

^eKandó Kálmán Faculty of Electrical Engineering, Óbuda University, Bécsi út 94-96, H-1034, Budapest, Hungary

^fMTA-WFK Lendület "Momentum" Semiconductor Nanoparticles Research Group, P.O. Box 49, H-1525 Budapest, Hungary

*gali.adam@wigner.hun-ren.hu

Elsevier use only: Received date here; revised date here; accepted date here

Abstract

In this study, we implement thiol termination on the surface of few-nanometer-sized silicon carbide (SiC) nanoparticles (NPs) to enable further applications, such as fluorescent biomarkers. Various spectroscopic techniques are employed to monitor the effectiveness of the surface treatment. Additionally, a thiol-Michael addition reaction is performed by conjugating 4-arm PEG-maleimide molecules to the thiol groups of SiC NPs, further demonstrating the reactivity of thiol-terminated SiC NPs. These thiolated SiC NPs, both with and without conjugated molecules, open new avenues in biotechnology.

Keywords: silicon carbide; nanoparticle; thiol termination; thiol-Michael addition; maleimide-PEG

1. Introduction

Nanoparticles have demonstrated immense potential across diverse fields, including energy production, environmental protection, information technology, food and agriculture, and biomedical

applications [1]. Among them, semiconductor nanoparticles hold particular promise due to their enhanced photocatalytic effects [2,3], tunable and stable photoemission [4–6]—suitable for applications ranging from bioimaging to light-emitting diodes (LEDs)—as well as improved photovoltaic efficiency and enhanced sensing capabilities. These advantages

* Corresponding author. Tel.: +36-1-392-2222; e-mail: gali.adam@wigner.hun-ren.hu.

arise from their high surface-to-volume ratio and unique quantum confinement and quantum mechanical properties. Additionally, the use of earth-abundant, non-toxic elements reduces toxicity risks and enhances accessibility, making them attractive for various applications. In this context, silicon carbide (SiC) emerges as a highly promising material due to its combination of numerous advantageous properties.

SiC is a widely studied indirect bandgap semiconductor [7] valued for its exceptional hardness and chemical resistance, making it ideal for advanced technical ceramics, electronics, automotive components, and precision tools [8]. Moreover, SiC can host point defect color centers [9,10] and qubits [11–13], expanding its potential for quantum technology applications [10,14–16].

SiC is also known for its low toxicity [17,18]. Fluorescent SiC nanoparticles (NPs) exhibit both hemocompatibility and biocompatibility [17]. When smaller than 10 nm, they display photoluminescence due to the combined effects of quantum confinement and surface states and have been successfully used for cell imaging [19,20] and dual-modality imaging, serving as both photoacoustic and photoluminescent contrast agents [21]. Incorporating SiC NPs into various matrices enhances material performance, including improving the mechanical strength and electrical conductivity of polymer nanocomposites [22] and enhancing the functionality of memory devices [23].

Structurally, the core of SiC NPs behaves as an inorganic crystal, while the surface is terminated with organic functional groups on the carbon side, including -COOH, -OH, and C=O moieties [24]. Without surface engineering, nanoparticle applications remain significantly limited, as surface termination is crucial for interactions with the surrounding environment. This is particularly relevant in biological systems, where surface chemistry dictates biomolecular interactions [25], accumulation sites, and toxicity profiles [26]. Additionally, surface properties influence dispersibility and stability in different matrices.

Engineering surface functionality enables the fabrication of nanosensors by sensitizing NPs to specific analytes, while also facilitating integration into conventional chemical processes, such as binding to various surfaces or biomolecules. Moreover,

surface chemistry directly influences the optical properties of SiC NPs [24,27,28], necessitating simultaneous monitoring of optical and physicochemical characteristics during surface functionalization verification.

Numerous methods for SiC NP functionalization have been reported. Our group has previously synthesized amino-terminated SiC NPs and conjugated them with bovine serum albumin (BSA) molecules [29,30]. Alekseev and coworkers have grafted alkene and amino groups onto SiC NPs [27]. However, to the best of our knowledge, thiol termination of SiC NPs has not yet been reported, despite its high potential.

Thiol (-SH) groups exhibit versatile chemical reactivity, enabling applications such as cross-linking through sulfide or disulfide formation [31], click chemistry in various reaction media [32], self-assembled monolayers (SAMs) [33], heavy metal scavenging [34], biosensing [35], biomedical applications [36] and the passivation and stabilization of noble metal nanoparticles for biological applications [37]. The ability to exploit the fluorescence properties of SiC-SH NPs across these diverse fields could open new avenues in sensor and imaging development.

In this study, we adopt an aqueous thiolation synthesis approach, previously used for nanodiamonds [38,39], to synthesize thiol-terminated SiC NPs. As-prepared SiC NPs exhibit oxygen-containing surface groups, similar to those found on nanodiamonds [24], and demonstrate superior dispersibility in polar solvents. However, SiC NP surface modification presents significant challenges due to the presence of silicon sites and their small size (~3 nm), requiring careful methodological adjustments to ensure successful functionalization.

Successful thiolization is confirmed using various analytical techniques, including Fourier-transform infrared spectroscopy (FTIR) and X-ray photoelectron spectroscopy (XPS), as well as maleimide conjugation via thiol-Michael addition click reaction [40,41]. Since thiols are highly sensitive to oxidation, they are often protected using stabilizing agents [42–45]. In this work, we employ polyethylene glycol (PEG) as a protective agent [42] conjugated with maleimide molecules—a process commonly referred to as PEGylation in the literature [46].

PEGylation is also widely applied in the biomedical field due to its ability to enhance drug solubility, improve nanoparticle stability, and extend circulation time by reducing renal clearance [47], while also minimizing protein adsorption [42]. Moreover, PEGylation has been utilized in targeted drug delivery [48,49] and the development of multi-arm PEG hydrogels for applications such as therapeutic agent delivery, tissue engineering [50], cell culture [51], 3D bioprinting [52], bone regeneration [53], and wearable biosensors [54].

Notably, multi-arm maleimide-PEG exhibits superior drug-loading capacity, improved drug solubility, and enhanced functional selectivity compared to its linear counterpart [53].

2. Materials and methods

2.1. Materials

The following materials were employed in this study: hydrofluoric acid (HF) (GPR Rectapur, VWR Chemicals), nitric acid (HNO₃) (GPR Rectapur, VWR Chemicals), ammonia solution (28%) (GPR Rectapur, VWR Chemicals), sodium borohydride (NaBH₄) (>98% powder, Sigma-Aldrich), hydrobromic acid (HBr) (48%, Acros Organics), acetic acid (HOAc) (96%, Reanal), thiourea (Reanal), sodium hydroxide (NaOH) (Analar Normapur, pellets, Sigma-Aldrich), sulfuric acid (H₂SO₄) (95%, Normapur, VWR Chemicals), and 4-arm-PEG-maleimide-10k (Sigma-Aldrich). All chemicals were used as received without further purification.

2.2. Instruments and characterizations

Conductivity measurements were done by using a CO 30 VWR conductivity meter.

FTIR spectra were acquired using a Bruker IFS 66v/S spectrometer operating at 3 mbar pressure, equipped with a Globar source and liquid nitrogen-cooled MCT (mercury cadmium telluride) detector. The samples were drop-cast on a single-side polished <100> Si wafer.

Photoluminescence (PL) spectra were recorded using Horiba Jobin-Yvon Fluorolog FL3-22 spectrophotometer equipped with a 450 W Xenon

lamp, an iHR-320 grating monochromator and an R928 photomultiplier tube. The samples were measured in a 10 × 10 × 40 mm quartz cuvette (Hellma 110QS, Jena, Germany).

Atomic force microscopy (AFM) imaging was performed using a Bruker Dimension Icon with Bruker MPP-111, 00-10 (Leipzig, Germany) probe equipment in tapping mode. 10 μL samples were drop-cast in a single-side polished <100> Si wafer and allowed to evaporate at room temperature. The scanning was processed around the dried droplets. 25 μm² area was scanned, and the height of at least 100 particles was measured for size distribution.

XPS measurements were conducted using a twin-anode X-ray source (Thermo Fisher Scientific, Waltham, MA, USA, XR4) and a hemispherical energy analyzer with a nine-channel multi-channeltron detector (SPECS-GROUP, Berlin, Germany, Phoibos 150 MCD). The base pressure in the analysis chamber was approximately 2 × 10⁻⁹ mbar. Mg K_α radiation (1253.6 eV) was used without monochromatization. Samples were drop-cast onto a niobium (Nb) substrate (GoodFellow GmbH, Hamburg, Germany). All spectra were corrected using the Nb 3d_{5/2} orbital of Nb₂O₅ at 207.1 eV and the C1s peak of adventitious carbon (C–C/C–H) at 284.8 eV. For the S2p orbital, a 1:2 ratio of S2p_{1/2}:S2p_{3/2} and an energy separation of 1.2 eV were used as split parameters. Peak fitting was performed using a GL30 function (Gaussian/Lorentzian, 30% Lorentzian character) with Shirley-type background subtraction.

High-resolution transmission electron microscopy (HRTEM), energy-dispersive spectroscopy (EDS), and electron diffraction analyses were performed using a Thermo TEM (Thermo Fisher) operated at 200 kV and equipped with spherical aberration (Cs) correction in the imaging system, providing a spatial resolution of 0.8 Å in HRTEM mode. Images were acquired using a 4 × 4 k Ceta camera with Velox software (Thermo Fisher). Samples were drop-cast onto a copper TEM grid (TED Pella) coated with an ultrathin lacey carbon layer and dried under an infra-LED lamp.

2.3. Synthesis of thiolated and PEGylated SiC NPs

SiC NPs were synthesized using the NPEGEC etching method [11,23,24,28,29,55–57]. Briefly, 5 g

of SiC microcrystals were etched in 40 mL of a 3:1 mixture of concentrated HF and HNO₃ at 150 °C in a PTFE-lined hydrothermal reactor. This process generated mesoporous layers on the microcrystals, which were subsequently disaggregated into nanocrystals via ultrasonication in an aqueous solution. The resulting nanocrystals were separated from the remaining microcrystals by centrifugation, yielding a colloidal solution of SiC NPs. The as-prepared SiC NPs are referred to as SiC-COOH.

The thiol-terminated SiC NPs were prepared in two steps. First, mild surface reduction was performed on SiC-COOH NPs (2 mg/mL). The pH of the NP suspension was adjusted to 14 by adding a few drops of NH₃ (25%) solution. Subsequently, NaBH₄ (0.08 g for 10 mL of NP suspension) was added, and the mixture was stirred at 80 °C for 12 hours. We refer to these reduced samples as SiC-OH. To create thiol-terminated NPs, 10 mL of a 2 mg/mL aqueous SiC-OH solution was placed in a 25 mL round-bottom flask and evaporated to dryness. Next, 3 mL of an HBr-HOAc solution (1:2 volume ratio) and 0.11 g of thiourea were added. The mixture was ultrasonicated at 80 °C for 3 hours at 37 kHz (Elmasonic P ultrasonicator). Then, 6 mL of a cold NaOH solution (7.5 M) was added to the hot mixture in an ice bath, followed by stirring at room temperature for 12 hours. To reduce the pH to 1–2, 96% H₂SO₄ was gradually added to the solution. Because of the high salt content precipitating during this step, the suspension was subsequently diluted and purified using a 1 kDa Pall Macrosep centrifugal filter until the permeate conductivity reached 0 μS. We label the thiol-functionalized samples as SiC-SH.

PEGylation was carried out by adding 3 mg of 4-arm maleimide-PEG to 0.5 mL of the SiC-SH suspension, followed by 12 hours of stirring. The mixture was then purified using a 1 kDa Pall Macrosep centrifugal filter. The resulting samples are referred to as SiC-S-PEG (Figure 1).

3. Results and discussion

The size and shape of the NPs before and after surface modification were determined by HRTEM (Figure 2) and AFM (Figure 3). The mean diameters derived from the AFM height profiles were 4.1 nm, 2.8

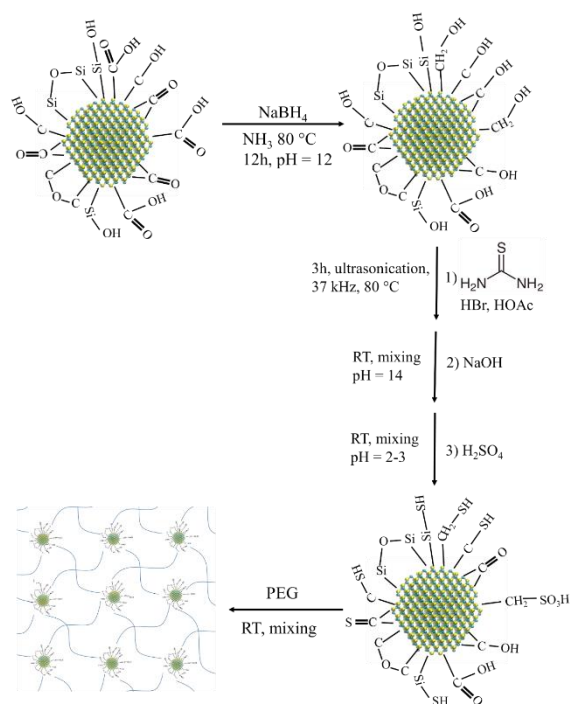


Figure 1. Synthesis of thiolated and PEGylated SiC NPs.

nm, and 5.4 nm for SiC-COOH, SiC-SH, and SiC-PEG, respectively. We attribute the observed size reduction following surface modification to the purification process, in which a substantial portion of

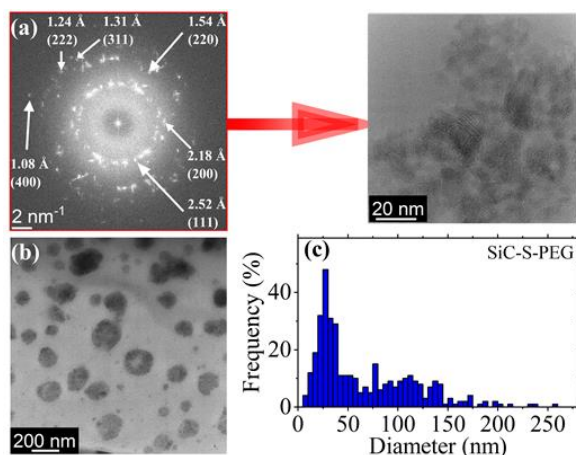
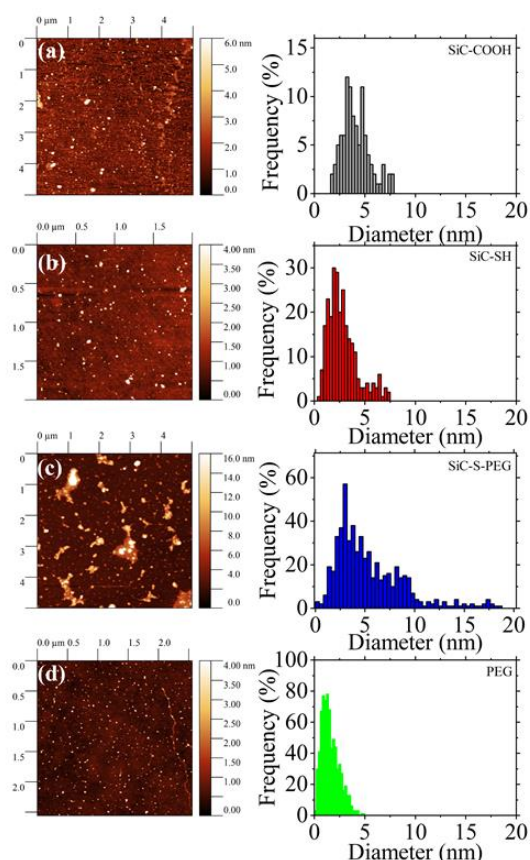


Figure 2. FFT image of SiC-SH NPs (a) measured on an ensemble of SiC-SH NPs (b), HRTEM image of SiC-S-PEG (c), the size distribution of SiC-S-PEG (d). Size distribution was calculated by measuring the diameters of 250 NPs from several areas.



the larger particles may have been removed. Electron
Figure 3. AFM images and size distributions of SiC-COOH (a), SiC-SH (b), SiC-S-PEG (c), and PEG (d) NPs.

diffraction performed on an assembly of SiC-SH particles confirmed that the material retained its SiC composition.

Notably, SiC-PEG exhibited a broader size distribution, and AFM images in Figure 3(c) revealed the presence of flat, wide structures. These results are consistent with HRTEM analyses presented in Figure 2(b). After PEGylation, the NPs tended to form larger structures (~ 30 nm), although the measured heights in AFM still corresponded to the original SiC-SH NPs. These findings suggest that the NPs are embedded in a soft polymer matrix, forming flattened, extended structures.

We also measured the polymer alone [Figure 3(d)], which has a mean size of ~ 1.6 nm, consistent with literature values for 10 kDa PEG molecules [58] that form a roughly spherical 3D structure.

The FTIR spectrum (Figure 4) of SiC-COOH NPs, SiC-SH NPs and PEG of SiC-COOH NPs primarily shows oxygen-related vibrational modes, including Si–O–Si/Si–O–C/C–O–C near 1100 cm^{-1} , –OH stretching around 3000 cm^{-1} , and C=O (carboxyl and other carbonyl) between 1600 and 1750 cm^{-1} [59]. After thiolation, significant changes were observed: the relative intensities of the C=O, COOH, and OH bands decreased markedly. In contrast, C–S, –S–H, and –S–S vibrations typically exhibit weak FTIR signals and were not detectable. A peak initially at 1437 cm^{-1} shifted to 1420 cm^{-1} (indicated with a dashed line), it may be associated with various overlapping vibrations (e.g., C–H, OH, sulfate). The notable reduction in OH content likely modifies hydrogen bonding, resulting in peak shifts and narrower features. However, partial oxidation of thiol groups to organic sulfates cannot be ruled out.

The FTIR spectrum of SiC-S-PEG shows characteristic peaks attributed to maleimide–PEG molecules [60–63], effectively masking the vibrations of other surface groups and rendering them undetectable by FTIR analysis [62].

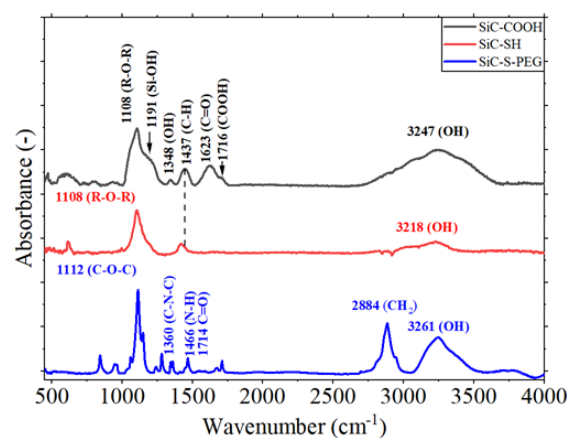


Figure 4. FTIR spectra of SiC-COOH (a), SiC-SH (b), and SiC-S-PEG (c) NPs. Spectra are vertically shifted for clarity

Survey XPS spectra and EDS analysis confirmed an increase in sulfur content following thiolation (Table 1).

Table 1. Elemental analysis of SiC-COOH, SiC-SH and SiC-S-PEG samples from XPS analysis. The values are in atomic concentrations (%).

sample	C	Si	O	S	N
SiC-COOH	51.3	3.5	44.8	0.1	0.3
SiC-SH	46.8	4.3	43.5	4.4	1.1
SiC-S-PEG	64.7	4.0	30.3	0.1	0.9

High-resolution C1s spectra also indicated a complex surface chemistry, with contributions from C-Si, C-C, C-O, C=O, and C-F in SiC-COOH NPs as plotted in Figure 5(a). Notably, the binding energies for C=O/C=S and C-O/C-S can overlap [64,65].

Table 2. Peak fitting parameters and component intensities of C1s photoelectron spectra of SiC-SH and SiC-S-PEG NPs. B.E. means binding energy, I.r. means intensity ratio.

sample	O-C=O		C-O/C-N C=O/C=S/ O=C-N-H		C=O/C=S		C-O/C-S		C-C/C-H		Si-C	
	B.E. (eV)	I.r. (%)	B.E. (eV)	I.r. (%)	B.E. (eV)	I.r. (%)	B.E. (eV)	I.r. (%)	B.E. (eV)	I.r. (%)	B.E. (eV)	I.r. (%)
SiC-COOH	290.1	11.6	-	-	288.3	21.3	286.3	9.1	284.8	50.4	283	1.5
SiC-SH	289.6	6.2	-	-	288.1	11	286.4	15.2	284.8	53.9	282.7	2.1
SiC-S-PEG	-	-	287.6	6.6	288.6	2.2	286.4	70.4	284.8	20.9	-	-

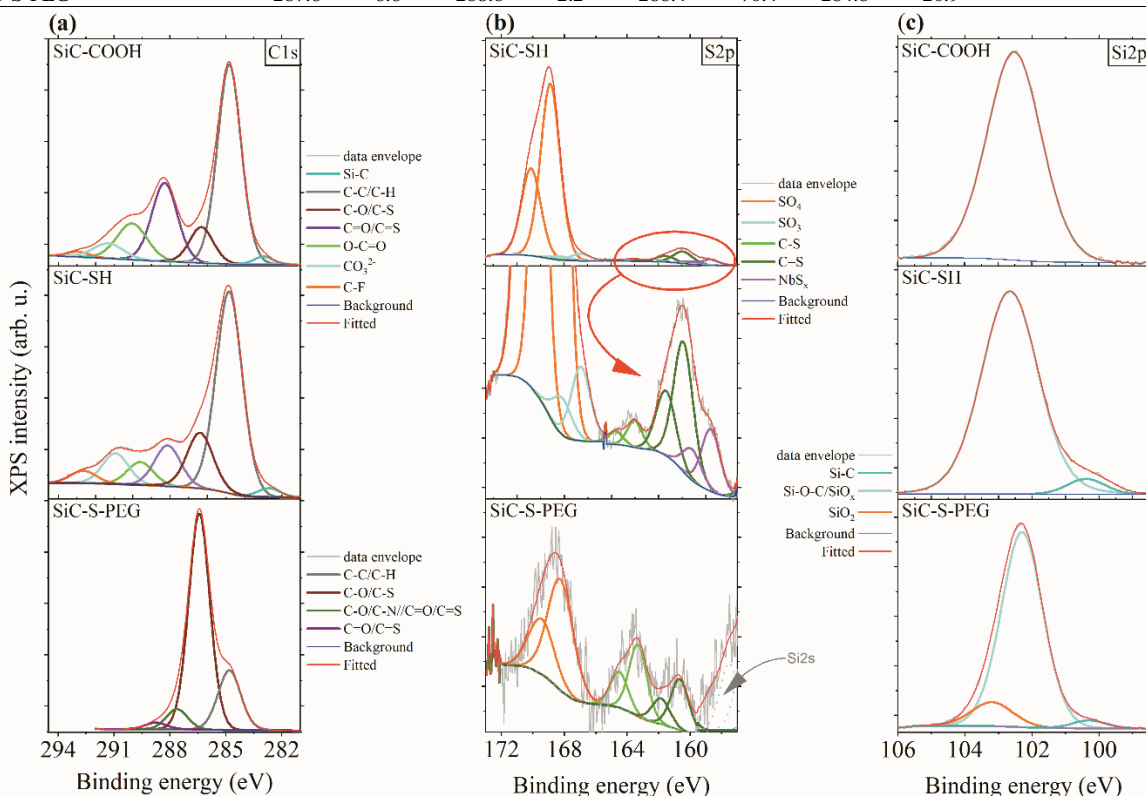


Figure 5. (a) C1s, (b) Si2p, (c) S2p photoelectron spectra of SiC-COOH, SiC-SH, SiC-S-PEG NPs, respectively

Following thiolation, the intensities of the O=C=O and C=O/C=S peaks decreased, while the C-O/C-S signal increased—consistent with the formation of C-S or C-O-S moieties, as supported by FTIR data showing a reduction in OH content.

In the C1s region of SiC-S-PEG, the peak structure aligns with PEG spectra reported in the literature, displaying C-O/C-N, C=O, and O=C-N-H components [66]. However, the relative intensity of C-O compared to C-C increased, consistent with findings where PEG is used as a protective agent [42].

The S 2p spectra for SiC-COOH, SiC-SH, and SiC-S-PEG indicate that a significant fraction of sulfur in SiC-SH was present in oxidized form (e.g., sulfates, O-S-O), although C-SH and C=S signals are also

detectable as shown in Figure 5(c). Thiol groups can be readily oxidized, which explains the relatively low concentration of free thiols. The presence of C=S may result from thione-thiol tautomerism [66,67].

Table 3. Peak fitting parameters and component intensities of S2p_{3/2} photoelectron spectra of SiC-SH and SiC-S-PEG NPs. B.E. means binding energy, I.r. means intensity ratio

sample	SO ₄		SO ₃		SH		C=S		NbS _x	
	B.E. (eV)	I.r. (%)	B.E. (eV)	I.r. (%)	B.E. (eV)	I.r. (%)	B.E. (eV)	I.r. (%)	B.E. (eV)	I.r. (%)
SiCSH	168.9	87	167	3.4	163.5	0.9	160.4	6	158.7	2.7
SiC-S-PEG	168.3	56.2	-	-	163.3	25.4	160.7	18.4	-	-

In SiC-S-PEG, oxidized sulfur species decrease, and the tautomeric equilibrium shifts toward thiol. Maleimides form stable thioether linkages with free thiols, and thioether binding energies can be comparable to those of thiols. Additionally, the PEG environment likely provides protection against oxidation, explaining both the observed shift in peak ratio and the reduction in oxidized sulfur.

Interestingly, an additional low-energy peak (<160 eV) was observed in the S2p region of SiC-SH but disappeared after PEGylation. While the S2p binding energies are usually higher than 160 eV, peaks at unusually low binding energies have been documented for S-Nb bonds [68,69]. We speculate that the niobium substrate used in the XPS analysis might form bonds with unprotected thiols, explaining the appearance of this low-energy peak and its disappearance upon PEGylation [70,71].

The Si2p spectra revealed three distinct bonding environments [Figure 5(b)]. In SiC-COOH NPs, only silicon-oxycarbide signals were consistently observed, in agreement with previous studies [29,72]. Upon thiolation (SiC-SH), the appearance of the Si-C peak suggested partial removal of the surface oxide layer. After PEGylation (SiC-S-PEG), a SiO₂ peak emerged, likely due to surface oxidation during the Michael addition reaction. Although Si-S bonds typically appear around ~102 eV, fitting the Si2p spectra using Si-C, Si-O, and Si-O_x components yielded a good match, with no significant increase in oxidized Si species after thiolation. This suggests that Si sites were not extensively involved in the thiolation reaction.

Table 4. Peak fitting parameters and component intensities of Si2p photoelectron spectra of SiC-SH and SiC-S-PEG NPs. B.E. means binding energy, I.r. means intensity ratio

Sample	SiO ₂		Si-O-C/SiO _x		Si-C	
	B.E. (eV)	I.r. (%)	B.E. (eV)	I.r. (%)	B.E. (eV)	I.r. (%)
SiC-COOOH	-	-	102.5	100	-	-
SiC-SH	-	-	102.6	94.4	100.3	5.6
SiC-S-PEG	103.3	22.1	102.2	75.3	100.3	2.6

Combining elemental analysis, FTIR, and XRD confirms successful surface modification of SiC NPs. The thiolated SiC surface reacts with maleimide groups, leading to PEGylated NPs that form a soft, polymer-based composite and protect residual thiol groups from further oxidation. We examined the photoluminescence (PL) of the NPs to assess the impact of this new surface chemistry on the optical behavior of luminescent SiC NPs (Figure 6). It is known that quantum confinement effects in SiC NPs are dominant for particle sizes above ~3 nm [57], while smaller NPs exhibit surface-related emissions. This emission partly originates from the HOMO (Highest Occupied Molecular Orbital) of the surface groups, which vary with surface termination [28]. Consequently, thiolation in the size regime studied here is expected to alter the PL spectrum compared to as-prepared SiC-COOH NPs.

Indeed, the PL of SiC-SH NPs was blue-shifted, similar to SiC-OH NPs (peak maximum at 435 nm) [28] although the shift was somewhat smaller. We attribute this difference to the higher electronegativity of –OH groups relative to –SH, wherein strongly negatively polarized –OH groups shift the HOMO downward more substantially. During PEG conjugation, SiC-S-PEG exhibited a further blueshift and a broader emission spectrum relative to SiC-SH, attributable to the formation of thioether bonds. These thioethers feature more negatively polarized sulfur than –SH, again lowering the HOMO, as well as possible contributions from PEG itself. The pronounced blue shift after PEGylation highlights the sensing potential of SiC-SH NPs, since sulfur bridge formation could be exploited when the –SH surface is used for target sensing.

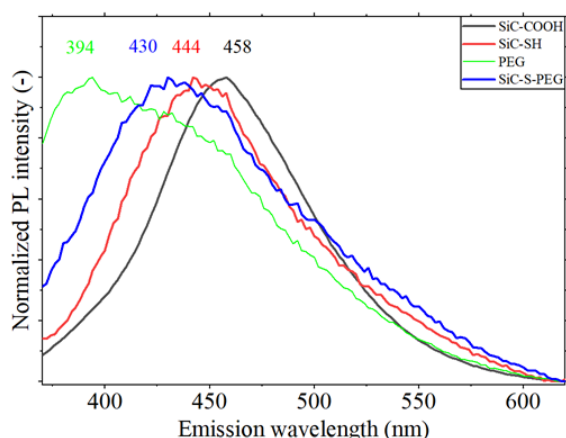


Figure 6. PL spectra of SiC-COOH (a), SiC-SH (b), PEG (c) and SiC-S-PEG (d) NPs

4. Conclusions

In this work, we successfully synthesized SiC NPs and demonstrated their thiolation and PEGylation as an effective strategy for tunable surface engineering. These modifications significantly affected the

photoluminescence properties of SiC NPs, indicating that both –SH groups and subsequent PEG conjugation can modulate optical emission by altering the nanoparticles' surface chemistry.

Data Availability Statement

All data available from the authors open reasonable requests.

Author Contributions

Conceptualization, D.B. and A.G.; methodology, P.R., O.K., S.L., Z.C. and D.B.; validation, D.B. and A.G.; formal analysis, O.K., P.R. and D.B.; data curation, P.R. and O.K.; funding acquisition, A.G.; investigation, P.R., O.K., and S.L.; project administration, A.G.; resources, A.G.; supervision, A.G.; writing—original draft, P.R. and A.G.; writing—review and editing, D.B., P.R. and A.G. All authors have read and agreed to the published version of the manuscript.

Funding

This study was supported by the Quantum Information National Laboratory sponsored by National Research, Development and Innovation Fund of Hungary (NKFIH) Grant No. 2022-2.1.1-NL-2022-00004 for the XPS and AFM investigations. The materials preparation was supported by the Ministry of Culture and Innovation of Hungary from NKFIH, financed under the TKP2021-NVA funding scheme (Project no. TKP2021-NVA-04). The HRTEM investigation was supported by the grant no. VEKOP-2.3.3-15-2016-00002 of the European Structural and Investment Funds. S. L. was supported by the Bolyai János Research Scholarship of the Hungarian Academy of Sciences and by the NKFIH grant ÚNKP-23-5-BME-448.

Declaration of conflicts of Interest

The authors declare no conflicts of interest.

Acknowledgments

The research reported in this paper and carried out at Wigner Research Centre for Physics is supported by the infrastructure of the Hungarian Academy of Sciences.

References

- [1] G. Speranza, Carbon Nanomaterials: Synthesis, Functionalization and Sensing Applications, *Nanomaterials* 11 (2021) 967. <https://doi.org/10.3390/nano11040967>.
- [2] P.V. Kamat, S. Jin, Semiconductor Photocatalysis: “Tell Us the Complete Story!,” *ACS Energy Lett.* 3 (2018) 622–623. <https://doi.org/10.1021/acsenerylett.8b00196>.
- [3] J. Kosco, M. Bidwell, H. Cha, T. Martin, C.T. Howells, M. Sachs, D.H. Anjum, S. Gonzalez Lopez, L. Zou, A. Wadsworth, W. Zhang, L. Zhang, J. Tellam, R. Sougrat, F. Laquai, D.M. DeLongchamp, J.R. Durrant, I. McCulloch, Enhanced photocatalytic hydrogen evolution from organic semiconductor heterojunction nanoparticles, *Nat. Mater.* 19 (2020) 559–565. <https://doi.org/10.1038/s41563-019-0591-1>.
- [4] A.L. Efros, L.E. Brus, Nanocrystal Quantum Dots: From Discovery to Modern Development, *ACS Nano* 15 (2021) 6192–6210. <https://doi.org/10.1021/acsnano.1c01399>.
- [5] M.A. Cotta, Quantum Dots and Their Applications: What Lies Ahead?, *ACS Appl. Nano Mater.* 3 (2020) 4920–4924. <https://doi.org/10.1021/acsanm.0c01386>.
- [6] M. Liu, N. Yazdani, M. Yarema, M. Jansen, V. Wood, E.H. Sargent, Colloidal quantum dot electronics, *Nat Electron* 4 (2021) 548–558. <https://doi.org/10.1038/s41928-021-00632-7>.
- [7] J.D. Blevins, Development of a World Class Silicon Carbide Substrate Manufacturing Capability, *IEEE Transactions on Semiconductor Manufacturing* 33 (2020) 539–545. <https://doi.org/10.1109/TSM.2020.3028036>.
- [8] H. Abderrazak, E.S.B. Hadj Hmi, Silicon Carbide: Synthesis and Properties, in: R. Gerhardt (Ed.), *Properties and Applications of Silicon Carbide*, InTech, 2011. <https://doi.org/10.5772/15736>.
- [9] S. Castelletto, B.C. Johnson, C. Zachreson, D. Beke, I. Balogh, T. Ohshima, I. Aharonovich, A. Gali, Room Temperature Quantum Emission from Cubic Silicon Carbide Nanoparticles, *ACS Nano* 8 (2014) 7938–7947. <https://doi.org/10.1021/nn502719y>.
- [10] A. Csóré, A. Gali, Point Defects in Silicon Carbide for Quantum Technology, in: *Wide Bandgap Semiconductors for Power Electronics*, John Wiley & Sons, Ltd, 2021: pp. 503–528. <https://doi.org/10.1002/9783527824724.ch17>.
- [11] D. Beke, J. Valenta, G. Károlyházy, S. Lenk, Z. Czigány, B.G. Márkus, K. Kamarás, F. Simon, A. Gali, Room-Temperature Defect Qubits in Ultrasmall Nanocrystals, *J. Phys. Chem. Lett.* 11 (2020) 1675–1681. <https://doi.org/10.1021/acs.jpcclett.0c00052>.
- [12] A. Gali, A. Gällström, N.T. Son, E. Janzén, Theory of Neutral Divacancy in SiC: A Defect for Spintronics, *Materials Science Forum* 645–648 (2010) 395–397. <https://doi.org/10.4028/www.scientific.net/msf.645-648.395>.
- [13] E. Janzén, A. Gali, P. Carlsson, A. Gällström, B. Magnusson, N.T. Son, The silicon vacancy in SiC, *Physica B: Condensed Matter* 404 (2009) 4354–4358. <https://doi.org/10.1016/j.physb.2009.09.023>.
- [14] G. Zhang, Y. Cheng, J.-P. Chou, A. Gali, Material platforms for defect qubits and single-photon emitters, *Applied Physics Reviews* 7 (2020) 031308. <https://doi.org/10.1063/5.0006075>.
- [15] N.T. Son, C.P. Anderson, A. Bourassa, K.C. Miao, C. Babin, M. Widmann, M. Niethammer, J. Ul Hassan, N. Morioka, I.G. Ivanov, F. Kaiser, J. Wrachtrup, D.D. Awschalom, Developing silicon carbide for quantum spintronics, *Applied Physics Letters* 116 (2020) 190501. <https://doi.org/10.1063/5.0004454>.
- [16] S. Castelletto, C.T.-K. Lew, W.-X. Lin, J.-S. Xu, Quantum systems in silicon carbide for sensing applications, *Rep. Prog. Phys.* 87 (2023) 014501. <https://doi.org/10.1088/1361-6633/ad10b3>.
- [17] *Silicon Carbide Biotechnology - 1st Edition*, (n.d.). <https://shop.elsevier.com/books/silicon->

- carbide-biotechnology/saddow/978-0-12-385906-8 (accessed January 17, 2024).
- [18] A. Oliveros, A. Guiseppi-Elie, S.E. Sadow, Silicon carbide: a versatile material for biosensor applications, *Biomed Microdevices* 15 (2013) 353–368. <https://doi.org/10.1007/s10544-013-9742-3>.
- [19] D. Beke, Z. Szekrényes, D. Pálfi, G. Róna, I. Balogh, P.A. Maák, G. Katona, Z. Czigány, K. Kamarás, B. Rózsa, L. Buday, B. Vértessy, A. Gali, Silicon carbide quantum dots for bioimaging, *Journal of Materials Research* 28 (2013) 205–209. <https://doi.org/10.1557/jmr.2012.296>.
- [20] M.O. de Vries, S. Sato, T. Ohshima, B.C. Gibson, J. Bluet, S. Castelletto, B.C. Johnson, P. Reineck, Fluorescent Silicon Carbide Nanoparticles, *Advanced Optical Materials* 9 (2021) 2100311. <https://doi.org/10.1002/adom.202100311>.
- [21] F. Chen, E.R. Zhao, T. Hu, Y. Shi, D.J. Sirbuly, J.V. Jokerst, Silicon carbide nanoparticles as a photoacoustic and photoluminescent dual-imaging contrast agent for long-term cell tracking, *Nanoscale Adv.* 1 (2019) 3514–3520. <https://doi.org/10.1039/C9NA00237E>.
- [22] H. Ahmed, A. Hashim, H. Abduljalil, Analysis of Structural, Electrical and Electronic Properties of (Polymer Nanocomposites/Silicon Carbide) for Antibacterial Application, *Egyptian Journal of Chemistry* 62 (2019) 767–776. <https://doi.org/10.21608/ejchem.2019.6241.1522>.
- [23] A. Mazurak, R. Mroczyński, D. Beke, A. Gali, Silicon-Carbide (SiC) nanocrystal technology and characterization and its applications in memory structures, *Nanomaterials* 10 (2020) 2387.
- [24] D. Beke, Z. Szekrényes, Z. Czigány, K. Kamarás, Á. Gali, Dominant luminescence is not due to quantum confinement in molecular-sized silicon carbide nanocrystals, *Nanoscale* 7 (2015) 10982–10988. <https://doi.org/10.1039/C5NR01204J>.
- [25] Q. Mu, G. Jiang, L. Chen, H. Zhou, D. Fourches, A. Tropsha, B. Yan, Chemical Basis of Interactions Between Engineered Nanoparticles and Biological Systems, *Chem. Rev.* 114 (2014) 7740–7781. <https://doi.org/10.1021/cr400295a>.
- [26] Y. Ji, Y. Wang, X. Wang, C. Lv, Q. Zhou, G. Jiang, B. Yan, L. Chen, Beyond the promise: Exploring the complex interactions of nanoparticles within biological systems, *Journal of Hazardous Materials* 468 (2024) 133800. <https://doi.org/10.1016/j.jhazmat.2024.133800>.
- [27] S. Alekseev, E. Shamatulskaya, M. Volvach, S. Gryn, D. Korytko, I. Bezverkhy, V. Iablokov, V. Lysenko, Size and Surface Chemistry Tuning of Silicon Carbide Nanoparticles, *Langmuir* 33 (2017) 13561–13571. <https://doi.org/10.1021/acs.langmuir.7b02784>.
- [28] D. Beke, T.Z. Jánosi, B. Somogyi, D.Á. Major, Z. Szekrényes, J. Erostyák, K. Kamarás, A. Gali, Identification of Luminescence Centers in Molecular-Sized Silicon Carbide Nanocrystals, *J. Phys. Chem. C* 120 (2016) 685–691. <https://doi.org/10.1021/acs.jpcc.5b09503>.
- [29] S. Czene, N. Jegenyés, O. Krafcsik, S. Lenk, Z. Czigány, G. Bortel, K. Kamarás, J. Rohonczy, D. Beke, A. Gali, Amino-Termination of Silicon Carbide Nanoparticles, *Nanomaterials* 13 (2023) 1953. <https://doi.org/10.3390/nano13131953>.
- [30] T. Bělinová, I. Machová, D. Beke, A. Fučíková, A. Gali, Z. Humlová, J. Valenta, M. Hubálek Kalbáčová, Immunomodulatory Potential of Differently-Terminated Ultra-Small Silicon Carbide Nanoparticles, *Nanomaterials* 10 (2020) 573. <https://doi.org/10.3390/nano10030573>.
- [31] S.-Y. Choh, D. Cross, C. Wang, Facile Synthesis and Characterization of Disulfide-Cross-Linked Hyaluronic Acid Hydrogels for Protein Delivery and Cell Encapsulation, *Biomacromolecules* 12 (2011) 1126–1136. <https://doi.org/10.1021/bm101451k>.
- [32] A.B. Lowe, Thiol-ene “click” reactions and recent applications in polymer and materials synthesis, *Polym. Chem.* 1 (2010) 17–36. <https://doi.org/10.1039/B9PY00216B>.
- [33] C. Vericat, M.E. Vela, G. Benitez, P. Carro, R.C. Salvarezza, Self-assembled monolayers of thiols and dithiols on gold: new challenges for a well-known system, *Chem. Soc. Rev.* 39 (2010) 1805–1834. <https://doi.org/10.1039/B907301A>.
- [34] G. Li, Z. Zhao, J. Liu, G. Jiang, Effective heavy metal removal from aqueous systems by thiol functionalized magnetic mesoporous silica, *J*

- Hazard Mater 192 (2011) 277–283. <https://doi.org/10.1016/j.jhazmat.2011.05.015>.
- [35] S. Xu, X. Han, A novel method to construct a third-generation biosensor: self-assembling gold nanoparticles on thiol-functionalized poly(styrene-co-acrylic acid) nanospheres, *Biosensors and Bioelectronics* 19 (2004) 1117–1120. <https://doi.org/10.1016/j.bios.2003.09.007>.
- [36] T. Potta, C. Chun, S.-C. Song, Chemically crosslinkable thermosensitive polyphosphazene gels as injectable materials for biomedical applications, *Biomaterials* 30 (2009) 6178–6192. <https://doi.org/10.1016/j.biomaterials.2009.08.015>.
- [37] S. Zhang, G. Leem, L. Srisombat, T.R. Lee, Rationally Designed Ligands that Inhibit the Aggregation of Large Gold Nanoparticles in Solution, *J. Am. Chem. Soc.* 130 (2008) 113–120. <https://doi.org/10.1021/ja0724588>.
- [38] M.-H. Hsu, H. Chuang, F.-Y. Cheng, Y.-P. Huang, C.-C. Han, J.-Y. Chen, S.-C. Huang, J.-K. Chen, D.-S. Wu, H.-L. Chu, C.-C. Chang, Directly Thiolated Modification onto the Surface of Detonation Nanodiamonds, *ACS Appl. Mater. Interfaces* 6 (2014) 7198–7203. <https://doi.org/10.1021/am500324z>.
- [39] B.A. Tkachenko, N.A. Fokina, L.V. Chernish, J.E.P. Dahl, S. Liu, R.M.K. Carlson, A.A. Fokin, P.R. Schreiner, Functionalized Nanodiamonds Part 3: Thiolation of Tertiary/Bridgehead Alcohols, *Org. Lett.* 8 (2006) 1767–1770. <https://doi.org/10.1021/ol053136g>.
- [40] B. Cengiz, N. Ejderyan, A. Sanyal, Functional polymeric coatings: thiol-maleimide ‘click’ chemistry as a powerful surface functionalization tool, *Journal of Macromolecular Science, Part A* 59 (2022) 443–455. <https://doi.org/10.1080/10601325.2022.2071725>.
- [41] C.E. Hoyle, A.B. Lowe, C.N. Bowman, Thiol-click chemistry: a multifaceted toolbox for small molecule and polymer synthesis, *Chem. Soc. Rev.* 39 (2010) 1355–1387. <https://doi.org/10.1039/B901979K>.
- [42] N. Gooch, V. Hlady, Two surface gradients of polyethylene glycol for a reduction in protein adsorption, *Surface Innovations* 3 (2015) 1–27. <https://doi.org/10.1680/sufi.15.00005>.
- [43] A. Corma, T. Ródenas, M.J. Sabater, Aerobic oxidation of thiols to disulfides by heterogeneous gold catalysts, *Chem. Sci.* 3 (2012) 398–404. <https://doi.org/10.1039/C1SC00466B>.
- [44] B J Lindberg, K Hamrin, G Johansson, U Gelius, A Fahlman, C Nordling, K Siegbahn, Molecular Spectroscopy by Means of ESCA II. Sulfur compounds. Correlation of electron binding energy with structure, *Phys. Scr.* 1 (1970) 286–298. <https://doi.org/10.1088/0031-8949/1/5-6/020>.
- [45] C.G. McKenas, J.M. Fehr, C.L. Donley, M.R. Lockett, Thiol–Ene Modified Amorphous Carbon Substrates: Surface Patterning and Chemically Modified Electrode Preparation, *Langmuir* 32 (2016) 10529–10536. <https://doi.org/10.1021/acs.langmuir.6b02961>.
- [46] D.P. Nair, M. Podgórski, S. Chatani, T. Gong, W. Xi, C.R. Fenoli, C.N. Bowman, The Thiol-Michael Addition Click Reaction: A Powerful and Widely Used Tool in Materials Chemistry, *Chem. Mater.* 26 (2014) 724–744. <https://doi.org/10.1021/cm402180t>.
- [47] B. Du, X. Jiang, Y. Huang, S. Li, J.C. Lin, M. Yu, J. Zheng, Tailoring Kidney Transport of Organic Dyes with Low-Molecular-Weight PEGylation, *Bioconjugate Chem.* 31 (2020) 241–247. <https://doi.org/10.1021/acs.bioconjchem.9b00707>.
- [48] J.H. Al Mahrooqi, V.V. Khutoryanskiy, A.C. Williams, Thiolated and PEGylated silica nanoparticle delivery to hair follicles, *International Journal of Pharmaceutics* 593 (2021) 120130. <https://doi.org/10.1016/j.ijpharm.2020.120130>.
- [49] E.A. Mun, P.W.J. Morrison, A.C. Williams, V.V. Khutoryanskiy, On the Barrier Properties of the Cornea: A Microscopy Study of the Penetration of Fluorescently Labeled Nanoparticles, Polymers, and Sodium Fluorescein, *Mol. Pharmaceutics* 11 (2014) 3556–3564. <https://doi.org/10.1021/mp500332m>.
- [50] J. Zhu, Bioactive Modification of Poly(ethylene glycol) Hydrogels for Tissue Engineering, *Biomaterials* 31 (2010) 4639–4656.

- <https://doi.org/10.1016/j.biomaterials.2010.02.044>.
- [51] S.R. Caliari, J.A. Burdick, A Practical Guide to Hydrogels for Cell Culture, *Nat Methods* 13 (2016) 405–414. <https://doi.org/10.1038/nmeth.3839>.
- [52] S. Piluso, G.A. Skvortsov, M. Altunbek, F. Afghah, N. Khani, B. Koç, J. Patterson, 3D bioprinting of molecularly engineered PEG-based hydrogels utilizing gelatin fragments, *Biofabrication* 13 (2021). <https://doi.org/10.1088/1758-5090/ac0ff0>.
- [53] S. Sun, Y. Cui, B. Yuan, M. Dou, G. Wang, H. Xu, J. Wang, W. Yin, D. Wu, C. Peng, Drug delivery systems based on polyethylene glycol hydrogels for enhanced bone regeneration, *Front. Bioeng. Biotechnol.* 11 (2023). <https://doi.org/10.3389/fbioe.2023.1117647>.
- [54] A.D. Masi, P.L. Scognamiglio, E. Battista, P.A. Netti, F. Causa, PEG-based cleavable hydrogel microparticles with controlled porosity for permiselective trafficking of biomolecular complexes in biosensing applications, *J. Mater. Chem. B* 10 (2022) 1980–1990. <https://doi.org/10.1039/D1TB02751D>.
- [55] D. Beke, Z. Szekrényes, I. Balogh, M. Veres, É. Fazakas, L.K. Varga, K. Kamarás, Z. Czígány, A. Gali, Characterization of luminescent silicon carbide nanocrystals prepared by reactive bonding and subsequent wet chemical etching, *Applied Physics Letters* 99 (2011). <https://pubs.aip.org/aip/apl/article-abstract/99/21/213108/150991> (accessed January 22, 2024).
- [56] N. Mukesh, B.G. Márkus, N. Jegenyés, G. Bortel, S.M. Bezerra, F. Simon, D. Beke, A. Gali, Formation of Paramagnetic Defects in the Synthesis of Silicon Carbide, *Micromachines* 14 (2023) 1517. <https://doi.org/10.3390/mi14081517>.
- [57] D. Beke, A. Fučíková, T.Z. Jánosi, G. Károlyházy, B. Somogyi, S. Lenk, O. Krafcsik, Z. Czígány, J. Erostyák, K. Kamarás, J. Valenta, A. Gali, Direct Observation of Transition from Solid-State to Molecular-Like Optical Properties in Ultrasmall Silicon Carbide Nanoparticles, *J. Phys. Chem. C* 122 (2018) 26713–26721. <https://doi.org/10.1021/acs.jpcc.8b07826>.
- [58] X. Dong, A. Al-Jumaily, I. Escobar, Investigation of the Use of a Bio-Derived Solvent for Non-Solvent-Induced Phase Separation (NIPS) Fabrication of Polysulfone Membranes, *Membranes* 8 (2018). <https://doi.org/10.3390/membranes8020023>.
- [59] L. Ivashchenko, A. Vasin, V. Ivashchenko, M. Ushakov, A. Rusavsky, Blue light emission from PECVD deposited nanostructured SiC, *MRS Proceedings* 910 (2006). <https://doi.org/10.1557/PROC-0910-A12-03>.
- [60] Y. Fu, W.J. Kao, In situ forming poly(ethylene glycol)-based hydrogels via thiol-maleimide Michael-type addition, *Journal of Biomedical Materials Research Part A* 98A (2011) 201–211. <https://doi.org/10.1002/jbm.a.33106>.
- [61] J.J. Khandare, A. Jalota-Badwar, S.D. Satavalekar, S.G. Bhansali, N.D. Aher, F. Kharas, S.S. Banerjee, PEG-conjugated highly dispersive multifunctional magnetic multi-walled carbon nanotubes for cellular imaging, *Nanoscale* 4 (2012) 837–844. <https://doi.org/10.1039/C1NR11540E>.
- [62] Y. Shtenberg, M. Goldfeder, A. Schroeder, H. Bianco-Peled, Alginate modified with maleimide-terminated PEG as drug carriers with enhanced mucoadhesion, *Carbohydrate Polymers* 175 (2017) 337–346. <https://doi.org/10.1016/j.carbpol.2017.07.076>.
- [63] J. Aramendia, L. Gomez-Nubla, M.L. Tuite, K.H. Williford, K. Castro, J.M. Madariaga, A new semi-quantitative Surface-Enhanced Raman Spectroscopy (SERS) method for detection of maleimide (2,5-pyrroledione) with potential application to astrobiology, *Geoscience Frontiers* 12 (2021) 101226. <https://doi.org/10.1016/j.gsf.2021.101226>.
- [64] D.M. Parker, A.J. Lineweaver, A.D. Quast, I. Zharov, J.S. Shumaker-Parry, Thiol-terminated nanodiamond powders for support of gold nanoparticle catalysts, *Diamond and Related Materials* 116 (2021) 108449. <https://doi.org/10.1016/j.diamond.2021.108449>.
- [65] K.-W. Jeon, Easily Processable, Highly Transparent and Conducting Thiol-Functionalized Reduced Graphene Oxides Langmuir-Blodgett Films, *Molecules* 26 (2021) 2686. <https://doi.org/10.3390/molecules26092686>.

- [66] W. Szaśiadek, I. Bryndal, M. Ptak, R. Lisiecki, T. Lis, J. Hanuza, Thione-thiol tautomerism in new 4-methyl-3-nitopyridine derivative in the solid state – X-ray, electron absorption and emission, IR and Raman studies discussed in term of quantum chemical DFT calculations, *Journal of Molecular Structure* 1286 (2023) 135531. <https://doi.org/10.1016/j.molstruc.2023.135531>
- [67] C. Abbehausen, R.E.F. de Paiva, A.L.B. Formiga, P.P. Corbi, Studies of the tautomeric equilibrium of 1,3-thiazolidine-2-thione: Theoretical and experimental approaches, *Chemical Physics* 408 (2012) 62–68. <https://doi.org/10.1016/j.chemphys.2012.09.019>.
- [68] In Situ Chemical Imaging of Solid-Electrolyte Interphase Layer Evolution in Li–S Batteries | *Chemistry of Materials*, (n.d.). <https://pubs.acs.org/doi/full/10.1021/acs.chemmater.7b00374> (accessed January 23, 2025).
- [69] R. Pai, V. Natu, M. Sokol, M. Carey, M.W. Barsoum, V. Kalra, Tuning functional two-dimensional MXene nanosheets to enable efficient sulfur utilization in lithium-sulfur batteries, *Cell Reports Physical Science* 2 (2021) 100480. <https://doi.org/10.1016/j.xcrp.2021.100480>.
- [70] C.J. Carmalt, C.W. Dinnage, I.P. Parkin, A.J.P. White, D.J. Williams, Synthesis of a Homoleptic Niobium(V) Thiolate Complex and the Preparation of Niobium Sulfide via Thio “Sol–Gel” and Vapor Phase Thin-Film Experiments, *Inorg. Chem.* 41 (2002) 3668–3672. <https://doi.org/10.1021/ic020097l>.
- [71] P. Gnanasekar, K.S. Ranjith, P. Manivel, Y.K. Han, J. Kulandaivel, Hierarchical NbS₂/MoS₂-Carbon Nanofiber Electrode for Highly Efficient and Stable Hydrogen Evolution Reaction at All Ranges of pH, *ACS Applied Energy Materials* 3 (2020) 6717–6725. <https://doi.org/10.1021/acsaem.0c00856>.
- [72] G. Károlyházy, D. Beke, D. Zalka, S. Lenk, O. Krafesik, K. Kamarás, Á. Gali, Novel Method for Electroless Etching of 6H–SiC, *Nanomaterials* 10 (2020) 538. <https://doi.org/10.3390/nano10030538>.